sciendo

DOI 10.2478/ama-2019-0013

acta mechanica et automatica, vol.13 no.2 (2019)

DEGRADATION OF FUNCTIONAL PROPERTIES OF PSEUDOELASTIC NiTi ALLOY UNDER CYCLIC LOADING: AN EXPERIMENTAL STUDY

Volodymyr IASNII*, Petro YASNIY*

*Department of Structural Mechanics, Ternopil Ivan Puluj National Technical University,
Ruska str. 56, 46001 Ternopil, Ukraine

v_iasnii@tntu.edu.ua, petroyasniy@gmail.com

received 14 March 2019, revised 3 June 2019, accepted 6 June 2019

Abstract: The influence of the cyclic loading on the functional properties of NiTi was studied. Cylindrical specimens with a diameter of 4 mm and a gage length of 12.5 mm were tested under uniaxial cyclic loading with control crosshead displacement at a temperature of 0°C. The dependences of the stress and strain range as well as dissipation energy on the number of loading cycles at different initial stress range were analysed. During the first 10 loading cycles, a rapid decrease in the strain range and energy dissipation was observed. Dissipation energy was invariant to the loading cycles' number at N > 20 cycles and to the stress range that did not exceed the martensite finish stress level, was within the same scatter band and can be described by the single dependence. With the stress range growth at N < 20 cycles from 509 to 740 MPa, the value of dissipation energy increases and that of relative dissipation energy decreases. Loss coefficient, which characterises material damping ability, significantly decreases during the first 10 loading cycles and remains practically unchanged up to the failure of the specimens. At the stabilisation area, the loss coefficient is almost non-sensitive towards the stress range.

Key words: pseudoelastic alloy, functional properties, dissipation energy, strain range, stress range

1. INTRODUCTION

Shape memory alloys (SMA) are the functional materials characterised by the shape memory effects and pseudoelasticity. Their application depends on the phase transformation temperatures, mechanical and functional properties, type of loading (static, cyclic, multiaxial and thermo-mechanical) (Sun L. et al., 2012; Hsu et al., 2019) and environment (Gamaoun et al., 2014; Iasnii et al 2019).

SMA are increasingly used in actuators (Nespoli et al., 2010), implants (Auricchio et al., 2015; Morgan, 2004; Chen and Thouas, 2015), and in earthquake engineering (Qiu and Zhu, 2017) because of the high ability to energy dissipation, as well as damping devices (Ozbulut et al., 2011; Yasniy et al., 2017; Torra et al., 2012; Isalgue et al., 2006) or other structural elements (Menna et al., 2015; Mohd Jani et al., 2014). As they are subjected to intense cyclic loading during operation, it is important to ensure their reliability and lifetime for low-cycle fatigue.

The balance between energy dissipation and structural fatigue lifetime should be reasonably taken into account whilst designing damping devices made of NiTi alloy.

It is known that with the increasing loading cycles, the SMA functional properties (pseudoelasticity) degrade. These properties can be characterised by the strain range, residual strain, dissipated energy (Kang et al., 2012; Predki, 2006, Iasnii and Yasniy, 2018; Eggeler et al., 2004) and loss factor. This factor represents the ratio of dissipated energy per cycle to maximum potential energy and was considered by Predki et al. (2006), Piedboeuf and Gauvin (1998) and Pan and Cho (2008). An increase in the average stress significantly reduces the residual strain of NiTi alloy under strain-controlled cyclic test (Kang et al., 2012). The residual strain is regarded as related to some oriented martensite, which is not transformed back into austenite during the reverse phase (Auricchio et al., 2003). Repeated changes in forward and reverse phases produce some defects in the material (Abeyaratne and Kin, 1997), resulting in localised internal stress (Tanaka et al., 1995) enabling two-way shape memory effect in SMA.

Particularly, residual and transformation hardening increase with the increase in the number of loading cycles and strain rates from 3.3×10^{-4} s^{-1} to $3.3\ 10^{-2}$ s^{-1} in super-elastic NiTi SMA microtube (50.32 % Ni) specimens during strain-controlled testing (Kan et al., 2016). The dissipation energy decreases with the increase in loading cycles. However, with the increase in the strain rate from 3.3×10^{-3} s^{-1} to 10^{-3} s^{-1}, the dissipation energy increases and further decreases. An increase in the residual strain is also observed at low-cycle fatigue of the NiTi wire under uniaxial tension (Moumni et al., 2009).

Therefore, in order to develop the behaviour models of structural elements and devices made of SMA, it is necessary to study the regularities of changing stress- and strain-based parameters, which characterise the functional properties.

The effect of loading range on the stress–strain curve, residual strain and dissipation energy of NiTi alloy was studied.

2. MATERIAL AND EXPERIMENTAL SETUP

Tests were carried out on commercial NiTi bar (8 mm, Wuxi Xin Xin glai Steel Trade Co., Ltd.).

The influence of the cyclic loading on the functional properties of Ni55,8Ti44,2 in the form of the rod of 8 mm in diameter was

DOI 10.2478/ama-2019-0013

studied. The chemical alloy composition stated in the certificate is 55.78% Ni; 0.005% Co; 0.005% Cu; 0.005% Cr; 0.012% Fe; 0.005% Nb; 0.032% C; 0.001% H; 0.04% O; 0.001% N; 44.12% Ti.

Phase transformation temperatures were identified using differential scanning calorimetry (DSC) by Q1000 TAI (Iasnii and Yasniy, 2018; Iasnii and Junga, 2018). Mechanical properties and influence of cyclic loading on the functional properties were studied at a temperature of 0°C under the uniaxial tension. Cylindrical specimens with a diameter of 4 mm and a gage length of 12.5 mm were machined from 8-mm rod (Iasnii and Yasniy, 2018). The tests were carried out on servo-hydraulic testing machine STM-10 (Yasniy et al., 2005) with automated control and data acquisition system under constant maximal crosshead displacement and sinusoidal load with a frequency of 0.5 Hz. Displacement ratio was $r = S_{min}/S_{max} = 0$, where S_{min}, S_{max} were the minimum and maximum value of crosshead displacement, respectively. During the tests at the first and following cycles at $S_{min} = 0$, the stress in the specimens becomes zero. This was provided by the structural feature of the grips. Force, crosshead displacement and elongation of the gauge length were recorded during the testing. Longitudinal strain was measured by Bi-06-308 extensometer produced by Bangalore Integrated System Solutions (BISS); maximum error did not exceed 0.1%. The crosshead displacement was determined by inductive Bi-02-313 sensor with an error not more than 0.1%. The tests were carried out in the chamber filled with ice and ice water. This provided the constant temperature of 0°C measured by chromel–alumel thermocouple mounted on the sample with an error not more than 0.5°C.

Literature data analysis shows that water has complex influence on the NiTi alloy fatigue behaviour. The low-cycle fatigue of NiTi SMA under the rotating–bending fatigue tests in air, in water and in silicone oil was studied by Tobushi et al. (2000). The influence of corrosion fatigue in water did not appear in the region of low-cycle fatigue. The fatigue life of NiTi alloy at an elevated temperature in air coincides with the fatigue life at the same elevated temperature in water.

No clear influence of the air or water environment on the fatigue life of NiTi alloys was found (Matsui et al., 2004). Rotating-bending fatigue tests were carried out in air and in water at room temperature and at 303 K.

Three conventional super-elastic NiTi instruments and two new CM wire instruments were subjected to rotational bending at the curvature of 35° in air and deionised water by Shen et al. (2012). The fatigue life of CM instruments was longer in water than in air.

Instruments of one brand of NiTi engine file were subjected to rotational bending either in air or under water and the number of revolutions to fracture was recorded using an optical counter and an electronic break-detection circuit by Cheung and Darvell (2007). A significant effect of the environmental condition on the LCF life was observed, water being more detrimental than air.

3. RESULTS AND DISCUSSION

The DSC (Fig. 1) curves show the martensitic–austenitic and austenitic–martensitic phase transformations occurring in SMA during the heating and cooling cycles relatively (Iasnii and Yasniy, 2018). Whilst heating the sample, the phase transformation takes place in the temperature range between −60.5°C and −38.7°C, and the transition temperature is −45.7°C. The reverse phase transformation during cooling is between −95.9°C and −69.4°C.

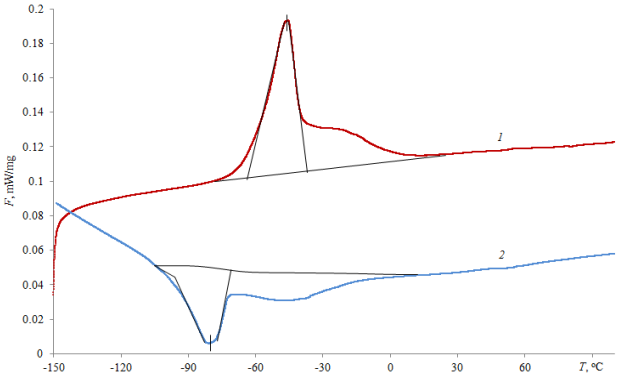

Fig. 1. Enthalpy change during phase transformation in SMA whilst heating (1) and cooling (2) (Iasnii and Yasniy, 2018)

Mechanical properties were determined according to ASTM F2516-14 standard, (2014) in ice water at 0°C which is higher than the austenitic finish temperature (A_f = −38.7°C): yield strength, $\sigma_{0,2}$ = 447 MPa, ultimate tensile strength, σ_{UTS} = 869 MPa (Iasnii and Yasniy, 2018).

Typical hysteresis loops for different values of the stress range and different number of load cycles (N = 1, 10, 20 cycles) are shown in Figure 2.

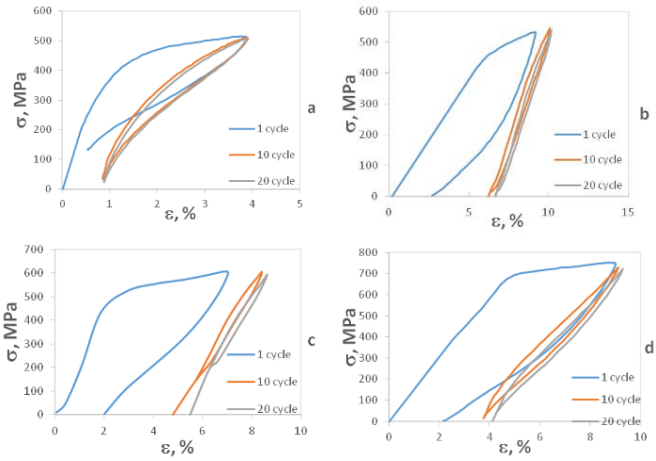

Fig. 2. Typical hysteresis loops for 1, 10 and 20 load cycles and stress range $\Delta\sigma_1$ = 509 MPa (a), 530 MPa (b), 605 MPa (c) and 748 MPa (d)

The dependences of the stress range (Fig. 3a) and the relative stress range (Fig. 3b) on the number of loading cycles at different initial values are shown in Figure 3. During the first cycle, all values of the initial stress range increase, that is, the material is strengthening. Then we can note weakening and stabilising regions followed by the decrease in the stress range. An exception is only for specimen with the initial stress range $\Delta\sigma_1$ = 748 MPa, where the value continuously decreases during testing.

Using the maximum stress related to the first cycle and ignoring the minor (up to 3%) deviation from the initial stress value, we can assume that the stress range remains constant and is equal to $\Delta\sigma_1$ during the testing (Fig. 3b).

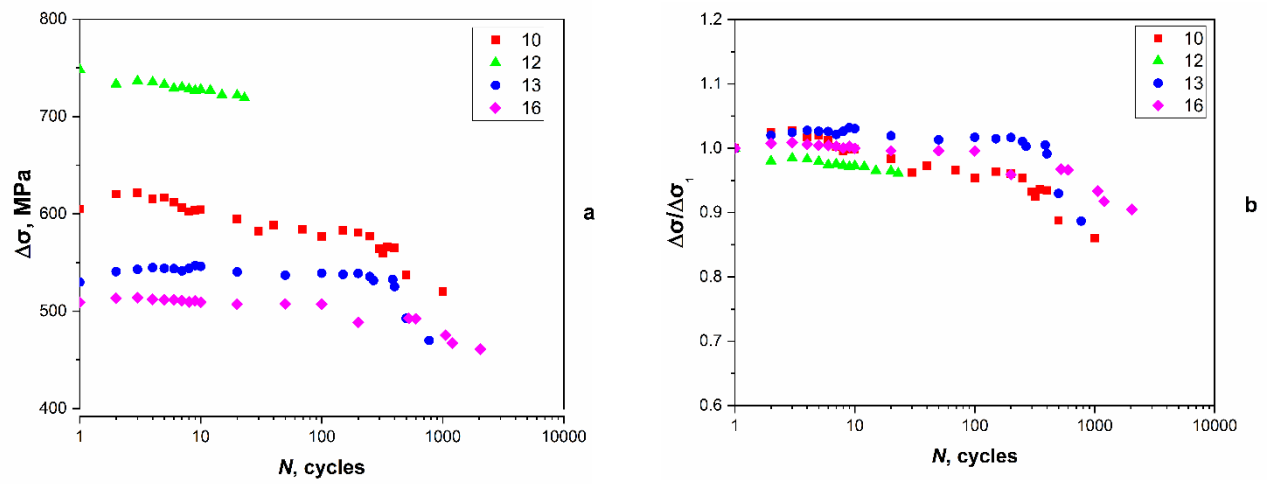

Fig. 3. Dependence of (a) the stress range and (b) the relative stress range on the number of loading cycles. $\Delta\sigma_1$ = 509 MPa (16), 530 MPa (13), 605 MPa (10) and 748 MPa (12). The specimen number is indicated in brackets

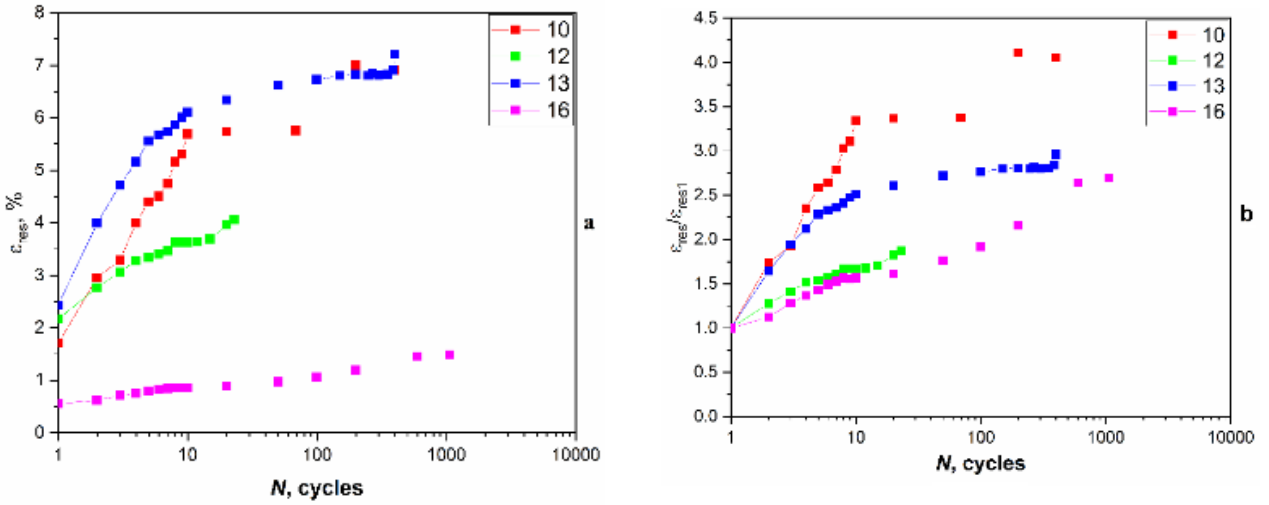

Fig. 4. Dependence of (a) the residual strain and (b) the relative residual strain on the number of loading cycles. $\Delta\sigma_1$ = 509 MPa (16), 530 MPa (13), 605 MPa (10) and 748 MPa (12)

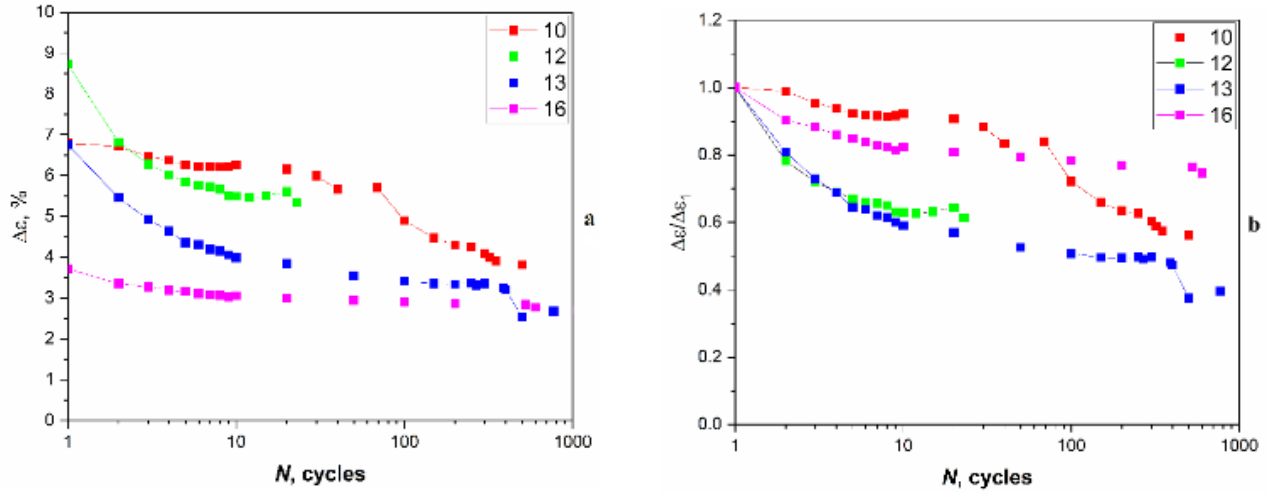

Fig. 5. Dependence of (a) the strain range and (b) the relative strain range on the number of loading cycles. $\Delta\sigma_1$ = 509 MPa (16), 530 MPa (13), 605 MPa (10) and 748 Mpa (12)

The functional properties of the pseudoelastic SMA can be characterised by residual strain. With the increase in the loading cycles, the residual strain (Fig. 4.a) and the relative residual strain $\overline{\varepsilon_r} = \varepsilon_r/\varepsilon_{r1}$, that is, the residual stress divided by the residual strain in the first loading cycle (Fig. 4b), grow. An increase in the stress range from 509 to 605 MPa increases the residual strain

DOI 10.2478/ama-2019-0013

that leads to the degradation of pseudoelasticity. However, with the further increase in the initial stress range to $\Delta\sigma_1$ = 740 MPa, the dependence of residual deformation on the number of loading cycles shifts below the same dependence for $\Delta\sigma_1$ = 605 MPa (Fig. 4a). The relative dependence of residual strain on the loading cycles' number at $\Delta\sigma_1$ = 740 MPa is the same as that at $\Delta\sigma_1$ = 509 MPa (Fig. 4b). The indicated inversion from the general law could be due to the fact that the strain range at $\Delta\sigma_1$ = 740 MPa in the first cycle is 8.7% that exceeds the maximum strain under which the superelastic effect is still visible.

The functional properties of the superelastic SMA can also be characterised by the strain range per cycle.

The dependences of residual strain (Fig. 5a) and relative residual strain (Fig. 5b) on the number of loading cycles for different stress range values in the first load cycle are shown in Figure 5.

For all values of the initial strain range during the first 10 loading cycles, a rapid decrease in the strain range, followed by the stabilisation area of strain range, or its less intensive reduction was observed.

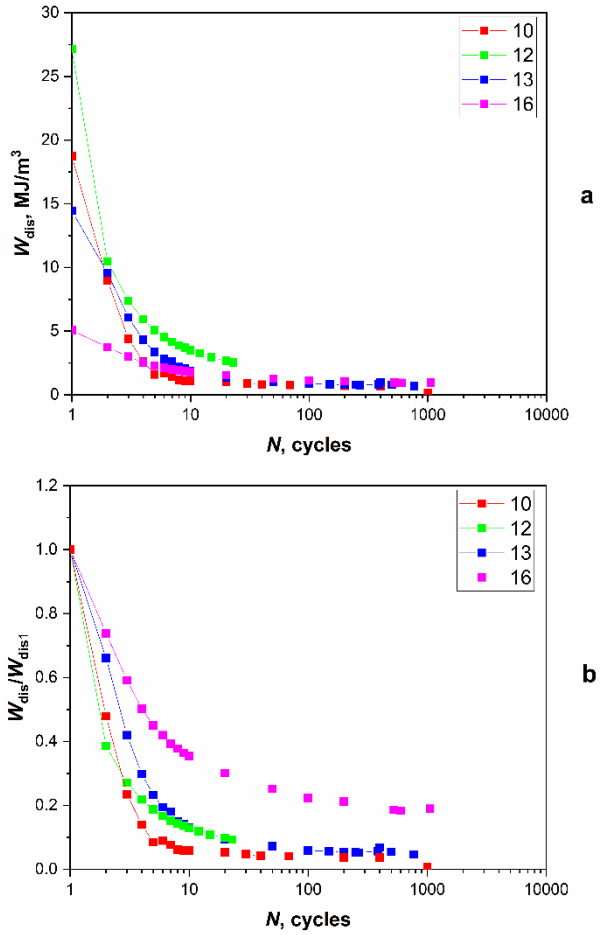

Fig. 6. Dependence of (a) dissipation energy and (b) relative dissipation energy on the number of load cycles. $\Delta\sigma_1$ = 509 MPa (16), 530 MPa (13), 605 MPa (10) and 748 MPa (12)

With the increasing in the stress range from 509 to 748 MPa, the strain range in the first cycle increase from 3.7% to 7.7% (Fig. 5b).

In general, the difference of strain range at a different stress level decreases with the increases in the number of loading cycles.

Dependences of dissipation energy and relative dissipation (energy) on the loading cycle number are given in Figure 6. For all values of the initial stress range as well as in the case of strain range, during the first 10–20 load cycles, a rapid decrease in the dissipation energy and relative dissipation energy passing into the stabilization region is observed. As the stress range increases in the first load cycle from 509 to 740 MPa, the value of the dissipation energy at the initial deformation stage increases up to 20 cycles (Fig. 6a) and that of the relative dissipative energy decreases before the failure specimens (Fig. 6b). The experimental values of the dissipation energy on the loading cycles' number (at N > 10 cycles) that are invariant to the stress range, which does not exceed the stress levels at which the martensite transformation completes, are located within the same scatter range and can be described by a single dependence.

The loss coefficient η, an effective parameter for measuring the device damping ability, is defined as the specific damping capacity per radian of the damping cycle (Pan and Cho, 2008):

$$\eta = \Delta W / (\pi (2W - \Delta W)) \quad (1)$$

where ΔW is the dissipated energy and W is the maximum potential energy of damping element.

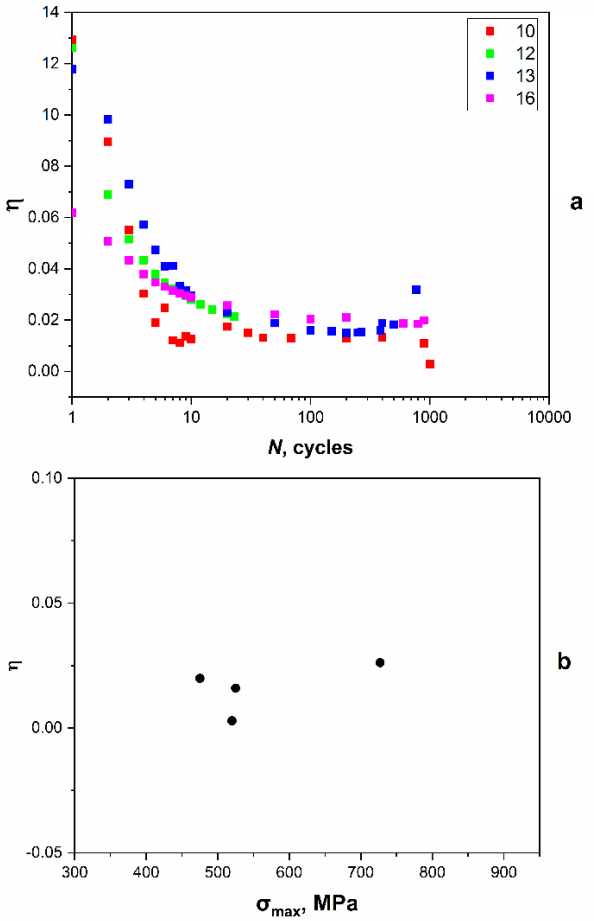

Fig. 7. The dependence of the loss coefficient on (a) the number of load cycles and (b) the stress range at $N = 0.5N_f$ – b. $\Delta\sigma_1$ = 509 MPa (16), 530 MPa (13), 605 MPa (10), 748 MPa (12)

At the initial stage of loading, with the increase in the cycles' number, the loss coefficient of NiTi alloy decreases, provided that the fastest drop in the loss coefficient is observed during the first 10 load cycles (Fig. 7a).

After 30–40 load cycles, the loss coefficient curves reach the plateau without regard to the applied value, the experimental points are located within the range of one scatter band of 0.01–0.02 (Fig. 7a).

According to the results of experimental investigations, the diagrams of cyclic alloy deformation for lifetime (Fig. 8) were built.

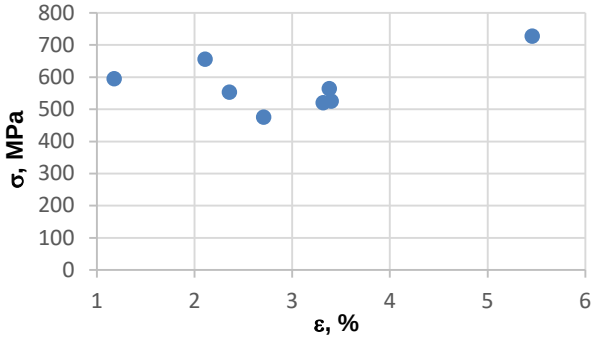

Fig. 8. Stress–strain curves of pseudoelastic NiTi alloy under cyclic loading for lifetime 0.5 N_f

These curves are important for the refined calculation of the stress–strain state of the structural elements made of SMA subjected to cyclic loading, as well as for the recalculation of power criteria of fatigue failure into deformation criteria and vice versa.

4. CONCLUSIONS

At the temperature higher than the temperature of the SMA, martensitic–austenitic transformation was completed under the conditions of controlled grips shifting; the dependence of the strain range on the cyclic operating time in general can be characterised by areas of strengthening, weakening and stabilisation.

The rapid decrease in the strain range observed during the first 10 loading cycles, without regard to the initial value of the strain range, is replaced by the stabilisation area that changes into the area of continuous strain range reduction of the extent of the strain resulting in specimen fracture. The residual strain and the strain range increase with the increase in the stress range for the same number of loading cycles.

Dissipation energy is invariant to the loading cycles' number at $N > 20$ cycles and to the strain range that does not exceed the martensite finish stress level, is within the same scatter band and can be described by the single dependence. With the stress range growth at $N < 20$ cycles from 509 to 740 MPa, the value of dissipation energy increases and that of the relative dissipation energy decreases before the failure specimens.

Loss coefficient, which characterizes material damping ability, significantly decreases during the first 10 loading cycles and remains practically unchanged up to the failure specimens. At the stabilisation area, the loss coefficient is almost non-sensitive towards the strain range.

REFERENCES

1. **Abeyaratne R., Kim S.-J.** (1997), Cyclic effects in shape-memory alloys: a one-dimensional continuum model, *International Journal of Solids and Structures*, 34(25), 3273-3289.
2. **Auricchio F., Boatti E., Conti M.** (2015), SMA Biomedical Applications, *Shape Memory Alloy Engineering*, Chapter 11, 307-341.
3. **Auricchio F., Marfia S., Sacco E.** (2003), Modelling of SMA materials: training and two way memory effect, *Computers & Structures*, 81, 2301-2317.
4. **ASTM F2516-14** (2014), Standard Test Method for Tension Testing of Nickel-Titanium Superelastic Materials.
5. **Chen Q., Thouas G.A.** (2015), Metallic implant biomaterials, *Materials Science and Engineering: R: Reports*, 87, 1-57.
6. **Cheung G.S.P., Darvell B.W.** (2007), Fatigue testing of a NiTi rotary instrument. Part 1: strain-life relationship, *International Endodontic Journal*, 40(8), 612-618.
7. **Eggeler G., Hornbogen E., Yawny A., Heckmann A., Wagner M.** (2004), Structural and functional fatigue of NiTi shape memory alloys, *Materials Science and Engineering: A*, 378(1-2), 24-33.
8. **Gamaoun F., Skhiri I., Bouraoui T., Ben Zineb T**. (2014), Hydrogen effect on the austenite–martensite transformation of the cycled Ni–Ti alloy, *Journal of Intelligent Materials Systems and Structures*, 25(8), 980-988.
9. **Hsu W.N., Polatidis E., Šmíd M., Van Petegem S., Casati N., Van Swygenhoven H.** (2019), Deformation and degradation of superelastic NiTi under multiaxial loading, *Acta Materialia*, 167, 149-158.
10. **Iasnii V., Junga R.** (2018), Phase Transformations and Mechanical Properties of the Nitinol Alloy with Shape Memory, *Materials Science*, 54(3), 406-411.
11. **Iasnii V., Nykyforchyn H., Tsyrulnyk O., Student O. (2019),** Specific features of deformation of the nitinol alloy after electrolytic hydrogenation, Materials Science, 54(4), 582-588.
12. **Iasnii V., Yasniy P., Lapusta Y., Shnitsar T.** (2018), Experimental study of pseudoelastic NiTi alloy under cyclic loading, *Scientific Journal of TNTU*, 92(4), 7-12.
13. **Isalgue A., Lovey F., Terriault P., Martorell F., Torra R., Torra V.** (2006), SMA for Dampers in Civil Engineering, *Materials Transactions*, 47(3), 682–690.
14. **Kan Q., Yu C., Kang G., Li J., Yan W.** (2016), Experimental observations on rate-dependent cyclic deformation of superelastic NiTi shape memory alloy, *Mechanics of Materials*, 97, 48-58.
15. **Kang G., Kan Q., Yu C., Song D., Liu Y.** (2012), Whole-life transformation ratchetting and fatigue of super-elastic NiTi Alloy under uniaxial stress-controlled cyclic loading, *Materials Science and Engineering: A*, 535(15), 228-234.
16. **Matsui R., Tobushi Y., Furuichi Y., Horikawa H.** (2004), Tensile Deformation and Rotating-Bending Fatigue Properties of a Highelastic Thin Wire, a Superelastic Thin Wire, and a Superelastic Thin Tube of NiTi Alloys, *Journal of Engineering Materials and Technology*, 126(4), 384.
17. **Menna C., Auricchio F., Asprone D.** (2015), *Shape Memory Alloy Engineering*, Elsevier.
18. **Mohd J., Leary M., Subic A., Gibson M.** (2014), A review of shape memory alloy research, applications and opportunities, Materials & Design, 56, 1078-1113.
19. **Morgan N.B.** (2004) Medical shape memory alloy applications - the market and its products, *Materials Science and Engineering: A*, 378(1-2), 16-23.
20. **Moumni Z., Zaki W., Maitournam H.** (2009), Cyclic Behavior and Energy Approach to the Fatigue of Shape Memory Alloys, *Journal of Mechanics of Materials and Structures*, 4(2), 395-411.
21. **Nespoli A., Besseghini S., Pittaccio S., Villa E., Viscuso S.** (2010), The high potential of shape memory alloys in developing miniature mechanical devices: A review on shape memory alloy mini-actuators. *Sensors and Actuators A: Physical*, 158, 149-160.
22. **Ozbulut O.E., Hurlebaus S., Desroches** R. (2011), Seismic response control using shape memory alloys: A review, *Journal of Intelligent Material Systems and Structures*, 22(14), 1531-1549.
23. **Pan Q., Cho C.** (2008), Damping property of shape memory alloys, *The 17th International Metallurgical and Materials Conference METAL*, 1-5.

24. **Piedboeuf M.C., Gauvin R.** (1998), Damping behaviour of shape memory alloys: strain amplitude, frequency and temperature effects, *Journal of Sound and Vibration*, 214(5), 885-901.
25. **Predki W., Klönne M., Knopik A.** (2006), Cyclic torsional loading of pseudoelastic NiTi shape memory alloys: Damping and fatigue failure, *Materials Science and Engineering: A*, 417(1-2), 182-189.
26. **Qiu C., Zhu S. (2017),** Shake table test and numerical study of self-centering steel frame with SMA braces, *Earthquake Engineering & Structural Dynamics*, 46(1), 117-137.
27. **Shen Y., Qian W., Abtin H., Gao Y., Haapasalo M.** (2012), Effect of environment on fatigue failure of controlled memory wire nickel-titanium rotary instruments, *Journal of Endodontics*, 38(3), 376-380.
28. **Sun L., Huang W.M., Ding Z., Zhao Y., Wang C.C., Purnawali H., Tang C.** (2012), Stimulus-responsive shape memory materials: A review, *Materials & Design*, 33, 577-640.
29. **Tanaka K., Nishimura F., Hayashi T., Tobushi H., Lexcellent C.** (1995), Phenomenological analysis on subloops and cyclic behavior in shape memory alloys under mechanical and/or thermal loads, *Mechanics of Materials*, 19(4), 281-292.
30. **Tobushi H., Nakahara T., Shimeno Y., Hashimoto T.** (1999), Low cycle fatigue of TiNi shape memory alloy and formulation of fatigue life, Journal of Engineering Materials and Technology, 122(2), 186-191.
31. **Torra V., Isalgue A., Auguet Sangra C., Carreras G.** (2012), The SMA: An Effective Damper in Civil Engineering that Smoothes Oscillations, *Materials Science Forum*, 706-2015, 2020-2025.
32. **Yasniy P., Hlado V., Hutsaylyuk V., Vuherer T.** (2005), Microcrack initiation and growth in heat-resistant 15Kh2MFA steel under cyclic deformation, *Fatigue & Fracture of Engineering Materials & Structures*, 28(4), 391-397.
33. **Yasniy P., Kolisnyk M., Kononchuk O., Iasnii V.** (2017), Calculation of constructive parameters of SMA damper, *Scientific Journal of TNTU*, 88(4), 7-15.